The Electrochemical Society
Advancing solid state & electrochemical science & technology

Three-Dimensional Performance Model for Oxygen Transport Membranes

View the article online for updates and enhancements.

Three-Dimensional Performance Model for Oxygen Transport Membranes

Andreas Häffelin,[a] Christian Niedrig,[a] Stefan F. Wagner,[a,z] Stefan Baumann,[b] Wilhelm A. Meulenberg,[b] and Ellen Ivers-Tiffée[a,c,*]

[a]*Institut für Werkstoffe der Elektrotechnik (IWE), Karlsruhe Institute of Technology (KIT), 76131 Karlsruhe, Germany*
[b]*Forschungszentrum Jülich, Institute of Energy and Climate Research IEK-1 Materials Synthesis and Processing, 52425 Jülich, Germany*
[c]*DFG Center for Functional Nanostructures, Karlsruhe Institute of Technology (KIT), 76131 Karlsruhe, Germany*

A three-dimensional finite element method (FEM) model that enables the performance simulation of mixed ionic-electronic conducting (MIEC) oxygen transport membranes (OTM) has been developed. In order to evaluate the influence of a porous functional layer on the membrane performance a numerical geometry generator was implemented that allows to create arbitrary porous microstructures. The 3D OTM model includes the spatially coupled physicochemical processes i) gas diffusion in the porous functional layer, ii) oxygen exchange at the feed-side between gas phase and MIEC material, iii) oxygen ion diffusion across the membrane, iv) oxygen excorporation at the permeate-side. The performed simulation carried out for the state-of-the-art MIEC composition $La_{0.6}Sr_{0.4}Co_{0.2}Fe_{0.8}O_{3-\delta}$ (LSCF) was validated with the help of oxygen permeation measurements carried out on an asymmetric LSCF thin-film OTM in the temperature range of 750...1000°C. The simulation results identified a surface exchange dominated regime for membrane thicknesses below 50 μm. While the application of a porous functional layer on the feed side could only increase the permeation flux by around 26%, the model demonstrates the significant improvement by a factor of two (for the given conditions) that can be achieved with a functional layer on the permeate side in case of a 20 μm thin-film membrane.

Oxygen transport membranes (OTM) are of great interest, e.g., for CO_2 capture and sequestration (CCS) in zero-emission fossil power plants, e.g.[1,2] To gain a highly CO_2 enriched exhaust gas, pure oxygen is used as the primary oxidant instead of ambient air ('Oxyfuel process'). In order to lower the energy consumption for oxygen production, the application of high temperature (600...900°C) oxygen-conducting membranes is promising compared to industrially established cryogenic processes. Mixed ionic-electronic conducting (MIEC) perovskite-type solid oxides, such as $La_{0.6}Sr_{0.4}Co_{0.2}Fe_{0.8}O_{3-\delta}$ (LSCF), e.g.,[3] or $Ba_{0.5}Sr_{0.5}Co_{0.8}Fe_{0.2}O_{3-\delta}$ (BSCF), e.g.,[4] represent state-of-the-art materials that facilitate high oxygen fluxes. The transfer of oxygen across the membrane is governed by the surface exchange reaction and the ambipolar diffusion through the dense bulk. For thick membranes oxygen permeation is mainly controlled by bulk diffusion. By reducing the thickness of the membrane, the oxygen flux will be increased. Hence a common proposed solution is to apply a supported thin-film membrane. However, upon reducing the thickness below a certain value (the "characteristic" membrane thickness typical of the material employed,[5] given by the ratio of oxygen diffusion constant and surface exchange coefficient), the diffusion processes become sufficiently fast, which leads to a change in the kinetic behavior: Ultimately, the surface reactions will become rate-determining for very thin membranes.[6] No significant enhancement of the oxygen flux is achieved by thinning the membrane any further if one cannot enhance the surface oxygen exchange.

However, an enhancement of the oxygen permeation can be achieved by modifying the membrane surfaces with a porous functional/catalytic layer that provides more surface area for the exchange of oxygen between the gas phase and the membrane material (the incorporation or the excorporation, respectively). In addition, binary gas diffusion in the pores of the support has to be considered kinetically as well in the case of very thin membrane layers.[7]

This concept has already been successfully applied to OTMs,[8] facilitating unprecedented oxygen flux values in the case of a 70 μm thick BSCF membrane covered with a 17 μm thick microporous BSCF layer[4] but also to solid oxide fuel cells (SOFCs) where nanoscaled thin-film cathodes made of the MIEC oxide $La_{0.6}Sr_{0.4}CoO_{3-\delta}$ with a nanoporous microstructure led to a large increase in oxygen surface reduction and thus the best performance of SOFC cathodes reported so far in literature.[9]

Computer-aided design of multiphase materials is a complex task which requires a powerful and flexible tool to evaluate the rate-determining steps on the performance. Different processes inside each phase and their mutual coupling through interfaces are to be considered. Previous work in literature has often been using simplified 1D models with an effective-medium approach for the performance prediction of porous MIEC membranes, e.g.,[10] In this paper, we present a three-dimensional (3D) finite element method (FEM) model for MIEC materials, based on the commercial software package COMSOL Multiphysics. It has previously successfully been applied to the case of an MIEC cathode in SOFCs, e.g.[11–13] The 3D OTM model includes a representation for the microstructure of a multiphase material and enables us to implement spatially different processes and couplings at interfaces.

Dimensioning the OTM for technical applications requires the calculation of the oxygen flux depending on the material composition, operating conditions and membrane design. As a figure of merit, the 3D OTM model calculates the oxygen flux through the MIEC membrane based on the respective chemical composition, assuming membrane thickness and structural parameters of the optional functional layer (layer thickness, particle size *ps*, and porosity ε), and additionally evaluates the microstructure-dependent penetration depth of the ionic current in the functional layer.

FEM Model

Processes and model implementation.— The OTM can be considered as a dense gastight ceramic sheet (bulk) separating two gas phases with different oxygen partial pressures p_{O_2}. The difference (gradient) of the oxygen partial pressure between the two separated sides (feed, permeate) is the driving force of the ionic flux through the membrane. The subsiding elementary processes i) gas diffusion, ii) oxygen incorporation, iii) bulk diffusion and (iv) oxygen excorporation (see Fig. 1) are taken into account in the 3D OTM model. With respect to the microscopic length scales of the model, isothermal conditions can be assumed. The two atmospheres A1 at the feed side and A2 at the permeate side are described by a high $p_{O_2,feed}$ and a low $p_{O_2,perm}$, respectively. Optionally, a porous functional layer can be applied on both sides of the dense membrane. The use of a functional layer

*Electrochemical Society Active Member.
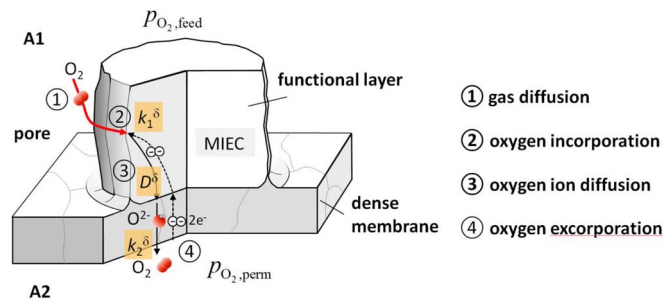[z]E-mail: stefan.wagner@kit.edu

Figure 1. Illustration of the processes (1) gas transport in the pores (including Knudsen diffusion), (2) surface exchange feed side (oxygen incorporation), (3) bulk diffusion and (4) surface exchange permeate side (oxygen excorporation).

provides additional surface area for the incorporation/excorporation of the oxygen from/into the gas phase.

At the feed side (A1) compressed air is supplied to increase the oxygen partial pressure (e.g., $p_{O_2,feed} = 1$ bar) and on the permeate side (A2) a technically realistic low-pressure oxygen atmosphere ($p_{O_2,perm} = 50$ mbar) was defined as boundary condition. According to the dusty gas model[14] the oxygen transport inside the pores is treated as a binary diffusion of oxygen and nitrogen and considers the interaction with the pore walls via a Knudsen diffusion term:

$$\nabla \cdot j_{gas}$$
$$= \nabla \cdot \left[-\frac{p}{RT} \cdot \left(\frac{1 - (1 - \sqrt{M_{O_2}/M_{N_2}})x_{O_2}}{D_{O_2 N_2}} + \frac{1}{D_{O_2}^K} \right)^{-1} \nabla x_{O_2} \right] = 0$$
$$[1]$$

Here $D_{O_2 N_2}$ denotes the binary diffusion coefficient,[15] x_{O_2} the local oxygen content (molar fraction), p the total gas pressure, R the universal gas constant, T the absolute temperature, and M_i the molar mass of species i. The Knudsen diffusion coefficient $D_{O_2}^K$[15] can be calculated with respect to the average pore radius d_P:

$$D_i^K = \frac{2}{3} d_P \cdot \sqrt{\frac{8 \cdot R \cdot T}{\pi \cdot M_i}}$$
$$[2]$$

Surface exchange at gas/membrane interface.— The oxygen exchange between the gas atmospheres and the membrane can be described by a surface exchange coefficient k^δ.[16] As this process depends on the oxygen partial pressure, a pO_2-dependent surface exchange coefficient is used on both sides of the membrane.

$$\vec{n} \cdot \vec{j}_{diff,O^{2-}}(\vec{x}) = -k^\delta(T, p_{O_2}) \cdot (c_{O^{2-},eq}(\vec{x}, t) - c_{O^{2-}}(\vec{x}))$$
$$[3]$$

Here $\vec{n}$ denotes the unit vector normal to the pore/MIEC interface. Inside the MIEC material, the diffusion of the oxygen ions can be described by the chemical diffusion coefficient D^δ.

As a model MIEC oxide the state-of-the-art cathode material $La_{0.6}Sr_{0.4}Co_{0.2}Fe_{0.8}O_{3-\delta}$ (LSCF) was considered in this study. For our modeling activities, k^δ and D^δ values for LSCF in dependency on the temperature and oxygen partial pressure were taken from Bouwmeester et al.[3]

Ionic bulk diffusion.— Due to the high electronic conductivity of LSCF ($\sigma_{el} \approx 300$ S$\cdot$cm^{-1} at $T = 800°C$), e.g.,[17] local electroneutrality can always be assumed. Hence the ionic diffusion in the MIEC phase can be attributed to a concentration gradient in the bulk and is described by Fick's law:

$$\vec{j}_{diff,O^{2-}}(\vec{x}) = -(D^\delta(T, p) \cdot \nabla c_{O^{2-}}(\vec{x}))$$
$$[4]$$

Assuming isothermal conditions and a low partial pressure dependency in the relevant range $50 \le p_{O_2} / mbar \le 1000$, $D^\delta(T)$ is used as a spatially constant value. In order to additionally consider impurities

in the bulk, an effective diffusion coefficient can be implemented in Eq. 4.

Total permeation flux.— The total oxygen permeation flux J_{O_2} can be calculated by the integration of the ionic current density with respect to the cross-sectional surface area A. J_{O_2} can be considered the figure of merit with respect to the membrane performance.

$$J_{O_2}(T, p_{O_2}) = \frac{1}{2} \cdot \int_A \vec{n} \cdot \vec{j}_{diff,O^{2-}}(\vec{x}) dA$$
$$[5]$$

Material parameters.— Considering Eqs. 3 and 4, the equilibrium oxygen ion concentration $c_{O^{2-},eq}$ together with the material parameters $k^\delta(T, p_{O_2})$ and $D^\delta(T, p_{O_2})$ are the only required external parameters entering the model. In order to enable simulations over a wide range of operating conditions literature data for LSCF from Bouwmeester et al.[3] was used to parametrize the model, namely chemical material parameters k^δ and D^δ obtained by conductivity relaxation measurements. For the implementation in the 3D OTM model, the equilibrium oxygen ion concentrations in dependency on the temperature and oxygen partial pressure in the gas phase have been calculated from oxygen nonstoichiometry measurements[3] by using Eq. 6 and were fitted with the linear functionality of Eq. 7. Hence, the model intrinsically includes the spatial coupling of the gas diffusion in the pore phase resulting in a local partial pressure and the interaction with the oxygen lattice concentration.

$$c_{O^{2-},eq} = \frac{3 - \delta}{3} \cdot c_{mc}$$
$$[6]$$

$$c_{O^{2-},eq}(T, p_{O_2}, \vec{x}) = g(T) \cdot \log(p_{O_2}(\vec{x})) + y(T)$$
$$[7]$$

Here c_{mc} denotes the concentration of oxygen lattice sites and δ the oxygen non-stoichiometry. For the calculation of c_{mc}, temperature-dependent values of the lattice constant for LSCF were used obtained by Wang et al.[18]

Model geometry.— The flexibility of a numerical model enables the use of various model geometries for the OTM performance simulation. Aside from the application of a bare membrane varying in dense bulk thickness, a porous functional layer can be applied on both surfaces of the membrane. Therefore a geometry generator was developed that allows the simulation of arbitrary porous microstructures. Hence, the 3D model intrinsically considers the thickness, pore size, porosity, and tortuosity of the functional layer. Fig. 2 shows the geometry, consisting of equally sized cubes that are symmetrically aligned. As the cubes are randomly assigned as pores or MIEC material,[19] all simulations are performed for ten individually generated microstructures (and then averaged) in order to avoid statistical errors. On top of the porous functional layer the pore phase is connected with a homogenous layer, representing the contact to the gas channel. As a boundary condition a constant oxygen partial pressure is applied at the gas inlet which is valid in case of a laminar flow in the adjacent gas channel.

Experimental

Sample preparation.— Both the membrane layer and the support were manufactured by tape casting using $La_{0.6}Sr_{0.4}Co_{0.2}Fe_{0.8}O_{3-\delta}$ (LSCF) powder (H. C. Starck, Germany) with an average particle size of 2.9 µm and a specific surface area of 10.7 m^2/g. The slurry preparation procedure was performed according to.[20] Two slurries were prepared with and without pore former, respectively. In order to create a percolating pore network within the support layer, rice starch Remy FG (BENEO-Remy, Belgium) with a particle size of 2 to 8 µm[21] was used. The rice starch content in the slurry was 20 wt% relative to the total solid content. Porosity was determined to be 30% by quantitative image analysis of polished cross sections. The slurry
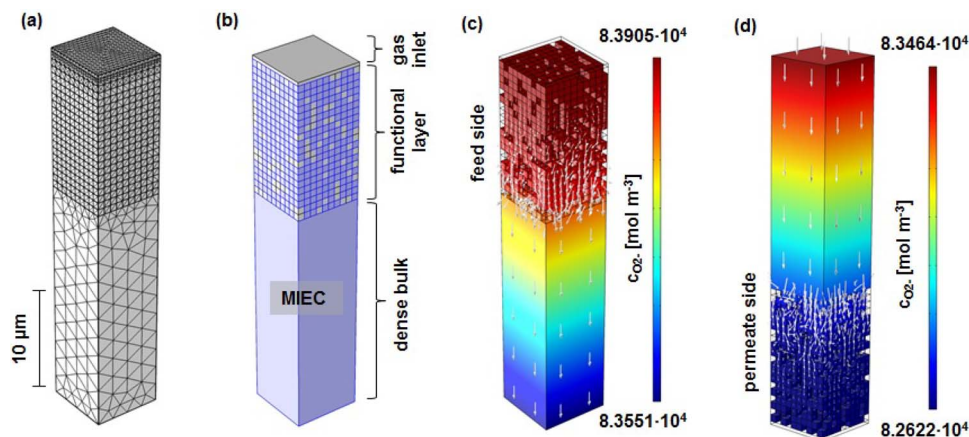
Figure 2. (a) FEM mesh and geometry generation. (b) Artificially generated MIEC functional layer on top of the dense membrane (blue) and pore phase (light gray). Simulated ionic concentration profile and current density distribution (arrows) of functional layer on the feed side (c) and permeate side (d) for LSCF at 800°C.

for the membrane layer did not contain any pore former leading to dense layers with porosity well below 3%. The membrane was prepared by sequential tape casting, where the membrane layer was cast first with a 0.1 mm casting gap. After drying, the support layer was cast on top of this layer with a casting gap of 1.9 mm. Samples were cut out from the dried green tape, debindered and subsequently co-fired in air at 1200°C for 5 h. The resulting microstructure is shown in Fig. 3. Membrane layer thickness is approx. 20 μm, whereas the total thickness is approx. 900 μm.

Oxygen flux measurements.— Oxygen permeation studies were carried out in a laboratory-scale quartz glass reactor. 250 ml/min air was fed into the oxygen-rich chamber, while 50 ml/min argon was used as the sweep gas on the permeate side. Both gases were fed in at atmospheric pressure. All streams were individually mass flow controlled. The temperature was measured by a thermocouple close to the membrane. The samples consisted of gastight supported LSCF membranes and membrane gas leak-free conditions were achieved using gold rings on both sides of the membrane, which were heated to 1010°C for 5 h immediately prior to the measurement. The permeate

was analyzed at steady-state by mass spectrometry (OmniStar, Pfeiffer Vacuum, Germany). Membrane gas leak-free conditions were ensured by continuously monitoring the nitrogen concentration in the product gas stream. The data reported here were achieved at steady-state after 3 h in the reaction stream. Oxygen permeation was determined in the temperature range of 750. . . 1000°C with the membrane layer and the support on the sweep and the feed side, respectively.

Simulation Results

The developed 3D OTM model aims to predict the membrane performance depending on the membrane design (bulk thickness, functional layer properties) and operating conditions (temperature, oxygen partial pressures). In order to validate the presented 3D OTM model, experimental permeation data is used for the comparison with the simulated OTM performance. Simulations were run to first identify the influence of the dense membrane thickness. Subsequently, the influence of an additional functional layer either on the feed side or on the permeate side were compared and evaluated in terms of porous microstructure design. Further simulations were run to demonstrate the influence of coupled rate-determining steps on the OTM performance.

Model validation.— The developed 3D OTM is validated by comparing the simulated oxygen permeation fluxes with measured permeation data obtained between 750. . . 1000°C on an asymmetric LSCF-supported dense LSCF membrane. Based on the SEM cross-section of the considered sample in Fig. 3, the following microstructure parameters are applied in the simulation: $d_{mem} = 20$ μm, $ps = 5$ μm, $\varepsilon = 30\%$. The feed oxygen partial pressure is constant at 210 mbar, whereas the oxygen partial pressure on the permeate side is dependent on the oxygen permeation rate and, hence, the temperature. It varies between 10 mbar at 750°C and 50 mbar at 1000°C. Fig. 4 shows the good agreement in the thermal behavior trend for various temperatures between 650. . . 800°C in case of the applied material parameters obtained by Bouwmeester et al.[3,d] However, it is worth mentioning that in literature a large scatter of the material parameters k^δ and D^δ can be found with deviations up to one order of magnitude[3,22–24] that are able to account for the deviation between the absolute values of the simulations and the experimental data. Thus, additional simulations with a variation of half a decade of the k^δ and D^δ values have been run and are taken to represent the confidence interval of the error bars shown in Fig. 4. Small discrepancies may also result from slight variations of the permeate-side partial pressure during the experiments.
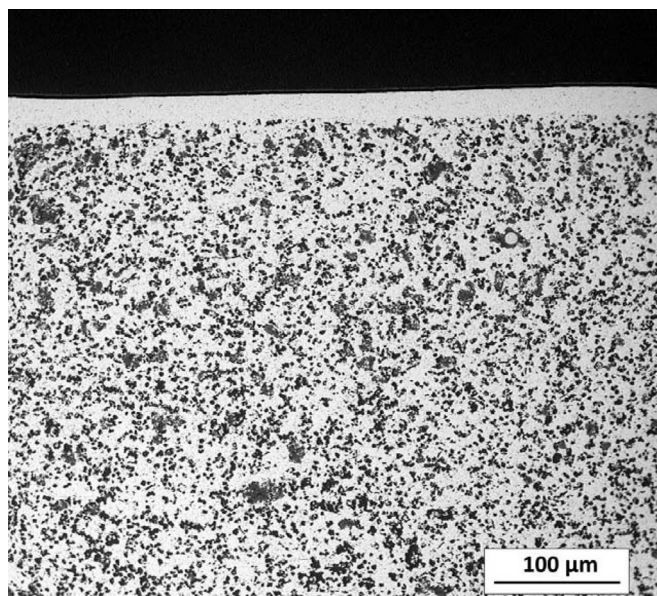

Figure 3. SEM image of a polished cross-section of the as-sintered asymmetric LSCF membrane.
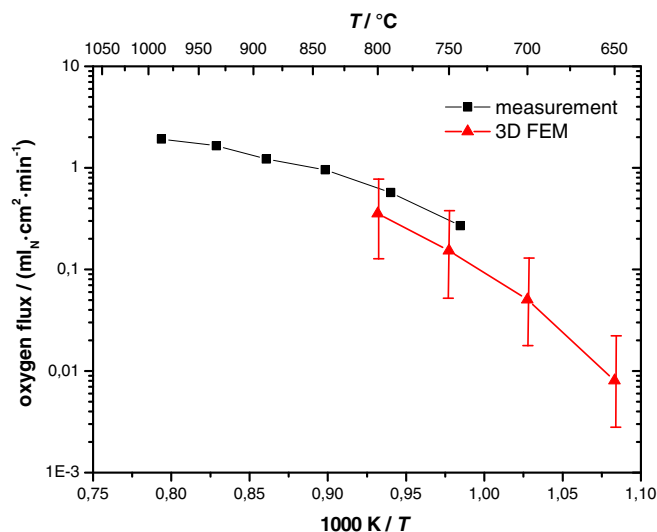
Figure 4. Validation of the simulated OTM performance ($d_{mem} = 20$ μm, $ps = 5$ μm, $\varepsilon = 30\%$, $p_{O_2,feed} = 0.21$ bar and $p_{O_2,perm} = 50$ mbar) with experimental permeation data.

Performance improvement by applying porous functional layers.— In order to enable performance predictions of a power-plant-integrated OTM, realistic operating conditions were used for the simulations. Therefore, on the feed side, compressed air is supplied ($p_{O_2,feed} = 1$ bar) while on the permeate side a constant partial pressure at the membrane surface of $p_{O_2,perm} = 50$ mbar is applied independently of the variation of permeation rate. Simulations were run to compare the improvement of the membrane performance with additional functional layers of variable particle size (i.e., mean grain diameters) and thickness on the feed, where the oxygen incorporation reaction occurs and on the permeate side to improve the oxygen excorporation reaction (cf. Fig. 2).

The simulations were run for different functional layer thicknesses up to 15 μm that consist of LSCF varying in particle sizes (ps), with $ps = [300, 600, 1000]$ nm and porosity $\varepsilon = 30\%$, respectively.

Fig. 5 shows the simulated oxygen flux (at 800°C) where the highest increase in permeation for both sides can be achieved for
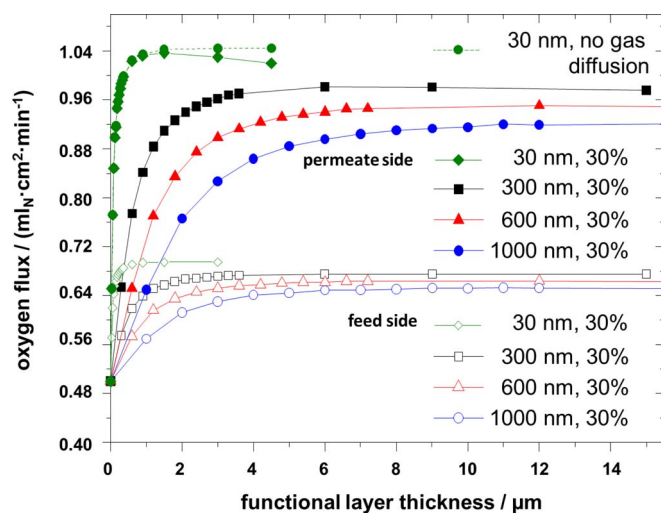
the smallest particle size of 30 nm. As the oxygen exchange occurs at the electrochemically active MIEC surface the largest volume-specific area is obtained for the smallest particle sizes and explains the performance variation as a result of the applied functional layer. Small deviations of the calculated oxygen flux by averaging over ten different microstructures can be detected and are attributed to statistical errors.

Additionally, it can be seen that for particle sizes of 1000 nm (300 nm) the increase in oxygen flux converges for a functional layer thickness of ∼ 8 μm (∼ 4 μm) which indicates the extension of the electrochemically active region. According to these simulation results for the applied operating conditions, the technical application should aim at a functional layer thickness as close to these values as possible. For particle sizes of 30 nm a functional layer thickness of only 1 μm already is sufficient. Additional functional layer material only contributes to the gas diffusion resistance and limits the membrane performance. However, this analysis shows that applying a functional layer on the feed side of a 20 μm thick membrane leads to a rather limited performance increase of less than 30%.

While the application of a functional layer on the feed side, hence, does not show a significant improvement on the membrane performance the simulated oxygen permeation flux can be increased by a factor of two, instead, by applying a functional layer on the permeate side (for the smallest particle size of 30 nm). This phenomenon can be related to the decrease of the surface exchange coefficient k^δ at low oxygen partial pressures,[3] thus identifying the oxygen excorporation as the overall performance-limiting mechanism. Therefore, the thickness of the electrochemically active region in a functional layer applied to the permeate side is enlarged to ∼12 μm (∼6 μm) in case of particle sizes of 1000 nm (300 nm). For a nm-sized porous functional layer with a particle size of 30 nm the highest oxygen flux can be achieved for a layer thickness of only slightly less than 2 μm.

In this case, however, gas diffusion limitation starts to influence oxygen flux for increasingly smaller particle sizes and increasing layer thicknesses – clearly visible for the case of the 30 nm-sized functional layer (solid green diamonds in Fig. 5).

This study shows that for the technical application a functional layer should be considered on the permeate side of the membrane to achieve a sufficient improvement. Particle size should be as small as technically feasible, while – to avoid gas diffusion limitation – layer thickness has to be engineered according to the maximum in obtainable oxygen flux (e.g., 2 μm for a particle size of 30 nm, cf. Fig. 5).

Considering that in the case of a thin-layer membrane on an oxygen-inert support (e.g., metal), a large part of the permeate-side surface area is blocked for oxygen surface exchange by the grains of the porous support material even emphasizes the role of the oxygen excorporation reaction as the rate-limiting process.

Dependency on functional-layer porosity.— To hand out optimized parameters for the technical design of the functional layer the oxygen permeation flux was calculated varying the porosity in a 12 μm thick porous microstructure with a homogenous particle size of 600 nm, applied onto the dense membrane ($d_{mem} = 20$ μm).

The simulation results given in Fig. 6 indicate an optimum porosity of 30% with a very slight variation in the defined tolerance interval in-between 25...40%. For porosities below 20% the percolation threshold is reached and the majority of pore space is not connected to the gas channel which results in a reduced permeation rate due to the electrochemically inactive regions.

Dependency on membrane thickness.— Fig. 7 shows the dependency of the oxygen permeation flux on the thickness of the dense membrane with and without a functional layer for temperatures between $T = 650...800$°C. It can be clearly seen that both the operating temperature as well as the membrane thickness have a large influence on the membrane performance. For a sufficiently thin membrane (thickness below 50 μm) the membrane predominantly operates in

Figure 5. Comparison of the performance improvement of functional layers on either feed or permeate side applied on a dense LSCF membrane with $d_{mem} = 20$ μm, varying in functional-layer thickness and particle size $ps = [300, 600, 1000]$ nm for porosity $\varepsilon = 30\%$, $T = 800$°C, $p_{O_2,feed} = 1$ bar and $p_{O_2,perm} = 50$ mbar.
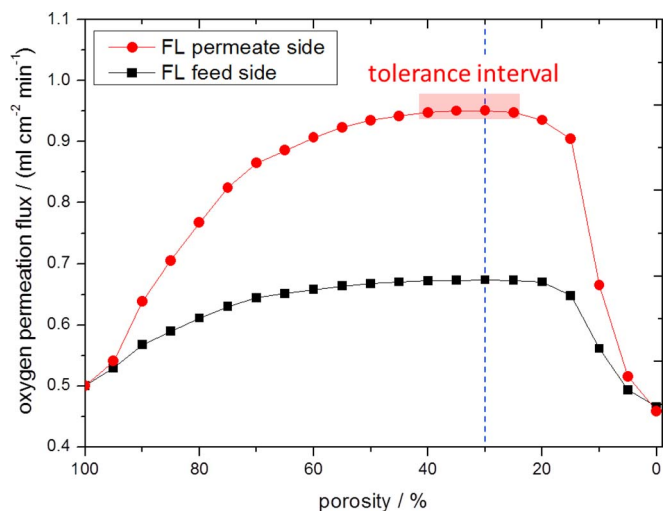
Figure 6. Variation of the functional layer porosity on the feed and on the permeate side for a 20 μm thick dense membrane and a functional layer thickness of 12 μm with particle size 600 nm at constant operating conditions ($T = 800°C$, $p_{O_2,feed} = 1$ bar, $p_{O_2,perm} = 50$ mbar).

a surface-controlled regime (Reg. I). Very recent technical developments have enabled production of dense and gastight membranes in the range of 40 μm and below, e.g.[25,26] Only for a sufficiently thin membrane (Reg. I), a considerable improvement of the performance can be achieved by the application of a functional layer. By comparing the difference in oxygen permeation with and without functional layer (Fig. 7), it becomes obvious that the flux improvement significantly decreases for increasing membrane thickness. In-between 50 μm and 110 μm membrane thickness oxygen transport is mixed surface/diffusion-controlled (Reg. II) which is in good agreement with the theoretically defined critical length $L_c = D^\delta/k^\delta$[5] amounting to 47 μm for LSCF at 800°C.[3] The final regime above 110 μm (Reg. III) shows low permeation fluxes due to the rate-determining ionic diffusion resistance and is obviously inadequate for technical OTMs.

Moreover, the simulated data highlights the large influence of the operating temperature. Compared to values at 650°C, a temperature increase to 800°C augments the permeation flux by a factor of approximately 16. Even for a relatively small temperature difference of

50 K between 750°C and 800°C a significantly higher permeation rate of ~ 40% can be achieved. This simulation result clearly points out that it is of main interest for the technical application of OTMs not only to manufacture thin-layer membranes (<50 μm), but also to ensure sufficiently high operating temperatures.

Identification of rate-determining steps.— The previous studies indicated a limited influence of the performance improvement that can be achieved with a functional layer on either feed or permeate side. Even though higher permeation rates could be observed for a functional layer on the permeate side, a convergence of the oxygen flux for functional layers thicker than around 13 μm occurred (cf. Fig. 5). The following simulations aim to demonstrate the interaction between the single rate-determining processes, assuming that the mechanical support of the membrane itself enables a sufficiently high permeation and does not contribute to any performance limitation. Therefore, different dense membrane thicknesses $d_{mem} = [1, 10, 100]$ μm were chosen and the surface-exchange kinetics on each side artificially improved by an enhancement factor λ between 1...100 representing the feasible influence of a functional layer applied to the surface of the membrane ($k_{i,sim}^\delta = \lambda \cdot k_{i,LSCF}^\delta$). In Fig. 8a the single coupled processes in an OTM are represented by a variable resistance network in similarity to the performed simulations.

The simulation results in Fig. 8b–8d point out that for decreasing membrane thickness a significant permeation-rate enhancement can be achieved for improved surface-exchange kinetics. In case of a 100 μm thick membrane in Fig. 8b the oxygen flux still converges even if the surface kinetics are strongly improved, due to the limitation caused by the ionic diffusion. For decreasing membrane thickness down to 1 μm in Fig. 8d it becomes obvious that the surface-exchange processes become rate-limiting and it is necessary to improve both the incorporation reaction and the excorporation reaction in order to enable a significant increase in membrane performance. However, the larger influence can be attributed to the oxygen excorporation reaction.

Consequently, it is of main interest for the realization of high-performance OTMs to primarily ensure thin-layer membranes with thicknesses down to 10 μm that additionally have the potential of an appreciable performance improvement achievable by applying a functional layer. If the membrane thickness cannot be reduced in the technical range of interest, an enhancement of the surface kinetics has only a limited influence on the membrane performance.
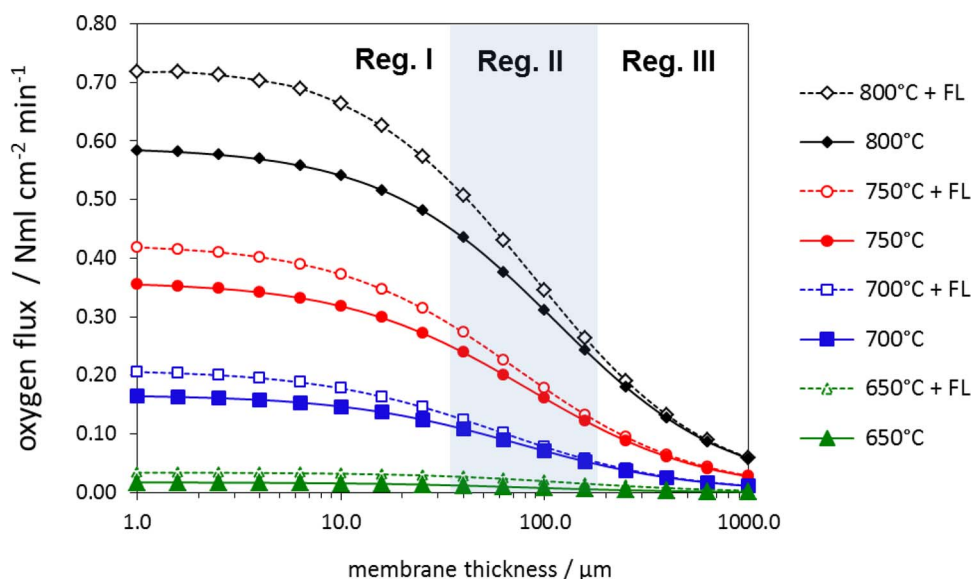

Figure 7. Oxygen permeation flux versus the dense membrane thickness for temperatures between $T = 650 \ldots 800°C$ and constant atmospheres $p_{O_2,feed} = 1$ bar, $p_{O_2,perm} = 50$ mbar. The influence of an additional feed-side functional layer (FL) can be seen from the comparison between solid and dashed curves.
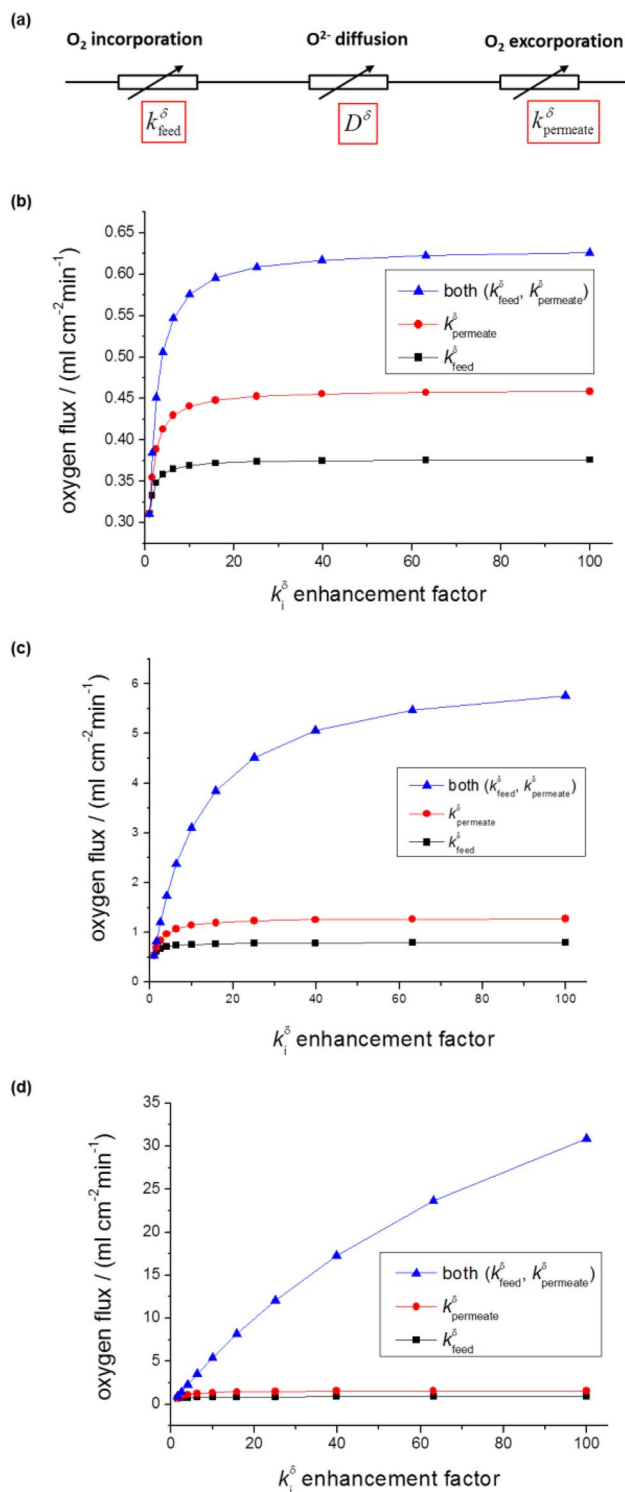
Figure 8. (a) Resistance network representing the coupled processes of oxygen incorporation, ionic diffusion and oxygen excorporation in the OTM and simulated oxygen permeation fluxes for dense membrane bulks varying in thickness d_{mem} (b) 100 μm, (c) 10 μm and (d) 1 μm in dependency on the artificially improved exchange kinetics.

Conclusions

A 3D OTM model that is able to predict the performance of a dense mixed-conducting membrane with an (optional) porous functional layer on the membrane surfaces has been developed. The spatially coupled physicochemical processes i) gas diffusion in the porous functional layer, ii) oxygen exchange at the feed side between the gas phase and the MIEC material, iii) oxygen ion diffusion across the membrane, iv) oxygen excorporation at the permeate side have been implemented in a finite-element method (FEM) framework. The 3D OTM model enables us to differentiate between material properties (k^δ, D^δ) and microstructural influences (thickness, porosity, and particle size) of the functional layer on the performance. By applying a porous functional layer on top of the membrane surface the performance should be strongly improved, as the additional surface area improves the rate of the oxygen exchange. As a figure of merit, the model hands out optimum design parameters such as sizing of the porous functional layer and thickness of the dense MIEC membrane, depending on chemical composition and operating conditions.

With the help of oxygen permeation measurements carried out at $750 \leq T /°\mathrm{C} \leq 1000$ on an asymmetric $La_{0.6}Sr_{0.4}Co_{0.2}Fe_{0.8}O_{3-\delta}$ (LSCF) tape-cast thin-film OTM (20 μm thickness) on a porous LSCF support, the OTM model could successfully be validated.

In order to simulate performance predictions of a power-plant integrated OTM, technical operating conditions were assumed in the model. The comparison of various functional layers depicted an optimum porosity of 30% for the functional layer. From the shown simulation results it can be seen that in case of a dense LSCF membrane with thicknesses below 50 μm, the surface exchange reaction is the rate-determining process for oxygen transport across the OTM. The consideration of a porous functional layer on the feed side in the first part of the study could only increase the permeation flux by less than 30% compared to the one of a bare membrane. In contrast, the inclusion of a functional layer on the permeate side of the membrane resulted in a performance improvement by a factor of almost two in case of a 20 μm thick membrane.

These simulation results clearly show that the performance of a thin-layer OTM made of LSCF is predominantly limited by the excorporation of oxygen and, thus, predict a significant performance enhancement by a custom-made porous functional layer applied to the permeate side.

References

1. M. Czyperek, P. Zapp, H. J. M. Bouwmeester, M. Modigell, K.-V. Peinemann, I. Voigt, W. A. Meulenberg, L. Singheiser, and D. Stöver, *Energy Procedia*, **1**, 303 (2009).
2. M. Czyperek, P. Zapp, H. J. M. Bouwmeester, M. Modigell, K. Ebert, I. Voigt, W. A. Meulenberg, L. Singheiser, and D. Stöver, *J. Membrane Sci.*, **359**, 149 (2010).
3. H. J. M. Bouwmeester, M. W. den Otter, and B. A. Boukamp, *J. Solid State Electrochem.*, **8**, 599 (2004).
4. S. Baumann, J. M. Serra, M. P. Lobera, S. Escolástico, F. Schulze-Küppers, and W. A. Meulenberg, *J. Membrane Sci.*, **377**, 198 (2011).
5. H. J. M. Bouwmeester and A. J. Burggraaf, in *The CRC Handbook of Solid State Electrochemistry*, P. J. Gellings and H. J. M. Bouwmeester, Editors, p. 481, CRC Press, Boca Raton, FL (1997).
6. H. J. M. Bouwmeester, H. Kruidhof, and A. J. Burggraaf, *Solid State Ionics*, **72**, 185 (1994).
7. P. Niehoff, S. Baumann, F. Schulze-Küppers, R. S. Bradley, I. Shapiro, W. A. Meulenberg, P. J. Withers, and R. Vaßen, *Separation and Purification Technology*, **121**, 60 (2014).
8. S. Baumann, W. A. Meulenberg, and H. P. Buchkremer, *J. European Ceramic Soc.*, **33**, 1251 (2013).
9. J. Hayd, L. Dieterle, U. Guntow, D. Gerthsen, and E. Ivers-Tiffée, *J. Power Sources*, **196**, 7263 (2011).

10. H. Deng, M. Zhou, and B. Abeles, *Solid State Ionics*, **74**, 75 (1994).
11. B. Rüger, A. Weber, and E. Ivers-Tiffée, *ECS Trans.*, **7**, 2065 (2007).
12. T. Carraro, J. Joos, B. Rüger, A. Weber, and E. Ivers-Tiffée, *Electrochim. Acta*, **77**, 315 (2012).
13. A. Häffelin, J. Joos, M. Ender, A. Weber, and E. Ivers-Tiffée, *J. Electrochem. Soc.*, **160**, F867 (2013).
14. R. Suwanwarangkul, E. Croiset, M. W. Fowler, P. L. Douglas, E. Entchev, and M. A. Douglas, *J. Power Sources*, **122**, 9 (2003).
15. E. L. Cussler, *Diffusion: Mass Transfer in Fluid Systems*, Cambridge University Press, Cambridge (1984).
16. J. Maier, *Physical Chemistry of Ionic Materials. Ions and Electrons in Solids*, John Wiley & Sons, Chichester UK (2004).
17. G. C. Kostogloudis and C. Ftikos, *Solid State Ionics*, **126**, 143 (1999).
18. S. R. Wang, M. Katsuki, M. Dokiya, and T. Hashimoto, *Solid State Ionics*, **159**, 71 (2003).
19. B. Rüger, J. Joos, A. Weber, T. Carraro, and E. Ivers-Tiffée, *ECS Trans.*, **25**, 1211 (2009).
20. J. M. Serra, J. Garcia-Fayos, S. Baumann, F. Schulze-Küppers, and W. A. Meulenberg, *J. Membrane Sci.*, **447**, 297 (2013).
21. E. Gregorová, W. Pabst, and I. Bohacenko, *J. European Ceramic Soc.*, **26**, 1301 (2006).
22. M. Søgaard, P. V. Hendriksen, T. Jacobsen, and M. Mogensen, in *Proc. 7th European Solid Oxide Fuel Cell Forum*, J. A. Kilner, Editor, B064 (2006).
23. P. Ried, E. Bucher, W. Preis, W. Sitte, and P. Holtappels, *ECS Trans.*, **7**, 1217 (2007).
24. A. Leonide, B. Rüger, A. Weber, W. A. Meulenberg, and E. Ivers-Tiffée, *J. Electrochem. Soc.*, **157**, B234 (2010).
25. F. Schulze-Küppers, S. Baumann, W. A. Meulenberg, D. Stöver, and H. P. Buchkremer, *J. Membrane Sci.*, **433**, 121 (2013).
26. N. Zotov, S. Baumann, W. A. Meulenberg, and R. Vaßen, *J. Membrane Sci.*, **442**, 119 (2013).